

# On the chemistry and distribution of HOC<sup>+</sup> in M 82

## More evidence for extensive PDRs

A. Fuente<sup>1</sup>, S. García-Burillo<sup>1</sup>, A. Usero<sup>1,2</sup>, M. Gerin<sup>3</sup>, R. Neri<sup>4</sup>, A. Faure<sup>5</sup>, J. Le Boulrot<sup>6</sup>, M. González-García<sup>6</sup>, J.R. Rizzo<sup>7</sup>, T. Alonso-Albi<sup>1</sup>, and J. Tennyson<sup>8</sup>

<sup>1</sup> Observatorio Astronómico Nacional (OAN), Apdo. 112, E-28800 Alcalá de Henares, Madrid, Spain

<sup>2</sup> Centre for Astrophysics Research, University of Hertfordshire, College Lane, Hatfield AL10 9AB, United Kingdom

<sup>3</sup> Laboratoire d'Etude du Rayonnement et de la Matière, UMR 8112, CNRS, Ecole Normale Supérieure et Observatoire de Paris, 24 rue Lhomond, F-75231 Paris Cedex 05, France

<sup>4</sup> Institut de Radioastronomie Millimétrique, 300 rue de la Piscine, F-38406 St Martin d'Hères Cedex, France

<sup>5</sup> Laboratoire d'Astrophysique Observatoire de Grenoble, BP 53, F-38041 Grenoble Cédex 9, France

<sup>6</sup> LUTH, Observatoire de Paris and Université Paris, 7 Place Jansen, F-92190 Meudon, France

<sup>7</sup> Laboratorio de Astrofísica Espacial y Física Fundamental, Apdo 78, E-28691 Villanueva de la Cañada, Madrid, Spain

<sup>8</sup> Department of Physics and Astronomy, University College London, Gower Street, London WC1E 6BT, United Kingdom

### ABSTRACT

**Context.** The molecular gas composition in the inner 1 kpc disk of the starburst galaxy M 82 resembles that of Galactic Photon Dominated Regions (PDRs). In particular, large abundances of the reactive ions HOC<sup>+</sup> and CO<sup>+</sup> have been measured in the nucleus of this galaxy. Two explanations have been proposed for such large abundances : the influence of intense UV fields from massive stars, or a significant role of X-Rays.

**Aims.** Our aim is to investigate the origin of the large abundances of reactive ions in M 82.

**Methods.** We have completed our previous 30m HOC<sup>+</sup> J=1→0 observations with the higher excitation HCO<sup>+</sup> and HOC<sup>+</sup> J=4→3 and 3→2 rotational lines. In addition, we have obtained with the IRAM Plateau de Bure Interferometer (PdBI) a 4'' resolution map of the HOC<sup>+</sup> emission in M 82, the first ever obtained in a Galactic or extragalactic source.

**Results.** Our HOC<sup>+</sup> interferometric image shows that the emission of the HOC<sup>+</sup> 1→0 line is mainly restricted to the nuclear disk, with the maxima towards the E. and W. molecular peaks. In addition, line excitation calculations imply that the HOC<sup>+</sup> emission arises in dense gas ( $n \geq 10^4 \text{ cm}^{-3}$ ). Therefore, the HOC<sup>+</sup> emission is arising in the dense PDRs embedded in the M 82 nuclear disk, rather than in the intercloud phase and/or wind.

**Conclusions.** We have improved our previous chemical model of M 82 by (i) using the new version of the Meudon PDR code, (ii) updating the chemical network, and (iii) considering two different types of clouds (with different thickness) irradiated by the intense interstellar UV field ( $G_0=10^4$  in units of the Habing field) prevailing in the nucleus of M 82. Most molecular observations (HCO<sup>+</sup>, HOC<sup>+</sup>, CO<sup>+</sup>, CN, HCN, H<sub>3</sub>O<sup>+</sup>) are well explained assuming that ~87% of the mass of the molecular gas is forming small clouds ( $A_v=5 \text{ mag}$ ) while only ~13% of the mass is in large molecular clouds ( $A_v=50 \text{ mag}$ ). Such small number of large molecular clouds suggests that M 82 is an old starburst, where star formation has almost exhausted the molecular gas reservoir.

**Key words.** galaxies: individual : M 82 — galaxies: nuclei — galaxies: starburst — ISM: molecules — ISM: abundances — radio lines: galaxies

## 1. Introduction

M 82 is one of the nearest and brightest starburst galaxies. Located at a distance of 3.9 Mpc, and with a luminosity of  $3.7 \times 10^{10} L_{\odot}$ , it has been the subject of continuum and line observations in virtually all wavelengths from X-rays to the radio domain. Several molecular line studies indicate that the strong UV field has heavily influenced the physical conditions, kinematics and chemistry in M 82 (Mao et al. 2000, Lord et al. 1996).

On the other hand, M 82 exhibits one of the largest optically visible outflows or “superwinds” in the local Universe. Superwinds are believed to be driven by the thermal and ram pressure of an initially very hot ( $T \sim 10^8 \text{ K}$ ), high pressure ( $P/k \sim 10^7 \text{ K cm}^{-3}$ ) and low density wind, itself created from merged supernovae remnants, and to a lesser extent by the stellar winds from massive stars. This very hot component is the re-

sponsible for the X-ray emission detected in this starburst galaxy (Strickland & Heckman 2007).

Back to the millimeter observations, M 82 is one of the most beautiful examples of how chemistry can help to the full understanding of the interstellar medium (ISM) of an external galaxy and the reverse, how the extragalactic research can push forward the chemistry comprehension. Our early HCO interferometric map using the PdBI showed that the M 82 nucleus is a giant photon-dominated region (PDR) of ~650 pc size. Furthermore the comparison between the HCO and H<sup>13</sup>CO<sup>+</sup> images suggested that the PDR chemistry is propagating across the M 82 nucleus (García-Burillo et al. 2002, hereafter Paper I). This propagation has to be understood in terms of the existence of different populations of clouds (different sizes, densities and temperatures) bathed by an intense UV field and with different spatial distribution across the M 82 disk. The densest clouds seem to be concentrated in two “hot spots” located  $\pm 15''$  from the center of the galaxy, E. and W. peaks (Mauersberger & Henkel 1991). Our

subsequent chemical study using the 30m telescope allowed us to put some restrictions to the ISM physical conditions. We observed the well known PDR tracers CN, HCN, HOC<sup>+</sup>, and CO<sup>+</sup> towards the M 82 nucleus (Fuente et al. 2005, 2006; hereafter Paper II and III). The high [CN]/[HCN] ratio and the detection of the reactive ions HOC<sup>+</sup> and CO<sup>+</sup> all across the galaxy disk proves the exceptionally high energetic conditions prevailing in the ISM of this galaxy. In extragalactic research, HOC<sup>+</sup> has only been detected in the active nucleus of NGC 1068 (Usero et al. 2004) and CO<sup>+</sup> has been only tentatively detected in Cygnus A (Fuente et al. 2000).

In Paper II and III, we modeled the chemistry in the M 82 disk using a PDR chemistry with an enhanced cosmic ray flux ( $4 \times 10^{-15} \text{ s}^{-1}$ ). Our best model accounted for the observed [CN]/[HCN] and [CO<sup>+</sup>]/[HCO<sup>+</sup>] ratios in the scenario of a highly fragmented interstellar medium in which small dense cores ( $n \sim 10^5 \text{ cm}^{-3}$ ,  $N_{\text{tot}} < 1.3 \times 10^{22} \text{ cm}^{-2}$ ) are bathed by an intense UV field ( $G_0 = 10^4$  Habing fields). This scenario is consistent with that proposed by Lord et al. (1996) based on observations of FIR forbidden lines. Melo et al. (2005) catalogued a total of 197 young massive clusters only in the starburst core. This incredible density of star clusters gives rise to a very unusual, highly energetic, and highly fragmented medium which is very different from anything in our Galaxy. The main drawback of our model is that it was unable to reproduce the large CO<sup>+</sup> column densities measured in this galaxy.

PDR chemistry is not the unique proposed scenario to explain the molecular chemistry in M 82. Spaans & Meijrenik (2007) suggested that the high CO<sup>+</sup> and HOC<sup>+</sup> column densities could be explained if their emission arises in a X-ray dominated region (XDR). Recently, van der Tak et al. (2008) detected the molecular ion H<sub>3</sub>O<sup>+</sup> in M 82 and concluded that the observed H<sub>3</sub>O<sup>+</sup> column densities were better explained by the enhanced cosmic ray PDR model than by the XDR model, however.

Our aim now is to investigate the origin, UV photon dominated or X-ray dominated chemistry, of the large abundance of reactive ions in M 82. In this Paper, we present a 4'' angular resolution image of the HOC<sup>+</sup> 1→0 line towards M 82, the first ever obtained in a Galactic or extragalactic source. In addition, we determine the excitation conditions of the gas emitting in HCO<sup>+</sup> and HOC<sup>+</sup>. Our results discard X-rays as the major driver of the reactive ions chemistry in M 82. With this information in our hands, we improve our chemical PDR model to account for the molecular abundances measured in M 82 thus far.

M 82 is one of the few galaxies in which we can resolve the individual molecular clouds and provides an excellent opportunity to study the PDR and/or XDR chemistries within a single object. This kind of studies are of paramount importance to establish extragalactic chemical patterns to discern between the influence of soft X-rays and UV photons on the chemistry of the most distant galaxies.

## 2. Observations

### 2.1. Single-dish observations

Observations of the J=3→2 and J=4→3 rotational lines of HCO<sup>+</sup> and HOC<sup>+</sup> were carried out using the 30m IRAM telescope located at Pico de Veleta (Spain) and the JCMT telescope at the Mauna Kea (Hawaii). In Table 1 we show a summary of all the observations used in this Paper. The 30m telescope observations were presented in Paper III.

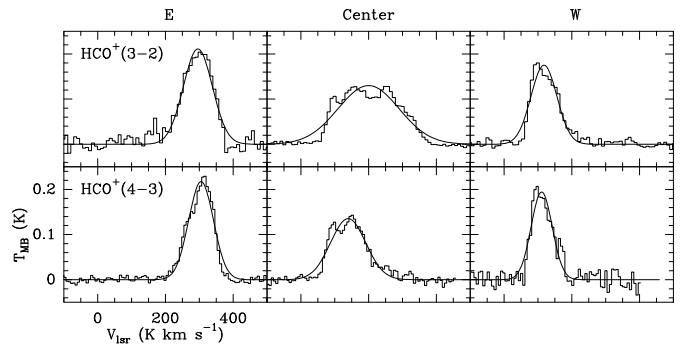


**Fig. 1.** Spectra of the J=3→2 and J=4→3 rotational lines of HCO<sup>+</sup> as observed with the JCMT. The W., Center and E. positions were observed in the two lines. Intensity scale is main beam temperature.

In Fig. 1 and Table 2 we show the observational results from the JCMT observations. All the lines were observed with a spectral resolution of 1 MHz. The frequencies of the rotational lines of both isotopomers, HCO<sup>+</sup> and HOC<sup>+</sup>, differ by less than 1 GHz. Therefore, we observed them simultaneously avoiding possible pointing and calibration errors in the measurement of the relative intensities.

### 2.2. Interferometric observations

We present high-angular resolution observations in the continuum at 3.3 mm and in the HOC<sup>+</sup> 1→0 rotational lines towards M 82. The observations were carried out with the IRAM<sup>1</sup> array at Plateau de Bure (PdBI) in 2005, May and December. The antennas were arranged in the C and D configurations providing an almost circular beam of 4.4'' × 3.6'' (natural weighting). We adjusted the spectral correlator to give a contiguous bandwidth of 1 GHz. The frequency resolution was set to 2.5 MHz (8.4 km/s). We subtracted the 3.3mm continuum emission using the GILDAS software package to generate the HOC<sup>+</sup> 1→0 image. The noise (rms) in the spectroscopic image is of ~1 mJy/beam.

In addition, a 3.3 mm continuum map was generated by averaging the channels free of line emission. Uniform weighting was applied to the measured visibilities producing a clean beam of 3.5'' × 2.7''. The noise (rms) in the 3.3mm continuum image is 0.3 mJy/beam.

The maps have not been corrected for primary beam attenuation which has at the frequency of HOC<sup>+</sup> a HPBW of 56''. The images are centered at the dynamical center of the galaxy, R.A. = 09:55:51.9, Dec = +69:40:46.90 (J2000).

## 3. Results

### 3.1. Single-dish observations

The HCO<sup>+</sup> 3→2 and 4→3 lines have been detected towards the three positions observed across the M 82 disk (see Fig. 1). We have not detected the HOC<sup>+</sup> 3→2 and 4→3 lines towards any of the observed positions using the JCMT. Gaussian fits to the HCO<sup>+</sup> 3→2 and 4→3 lines and upper limits to the HOC<sup>+</sup> lines are given in Table 2.

<sup>1</sup> IRAM is supported by INSU/CNRS (France), MPG (Germany) and IGN (Spain).

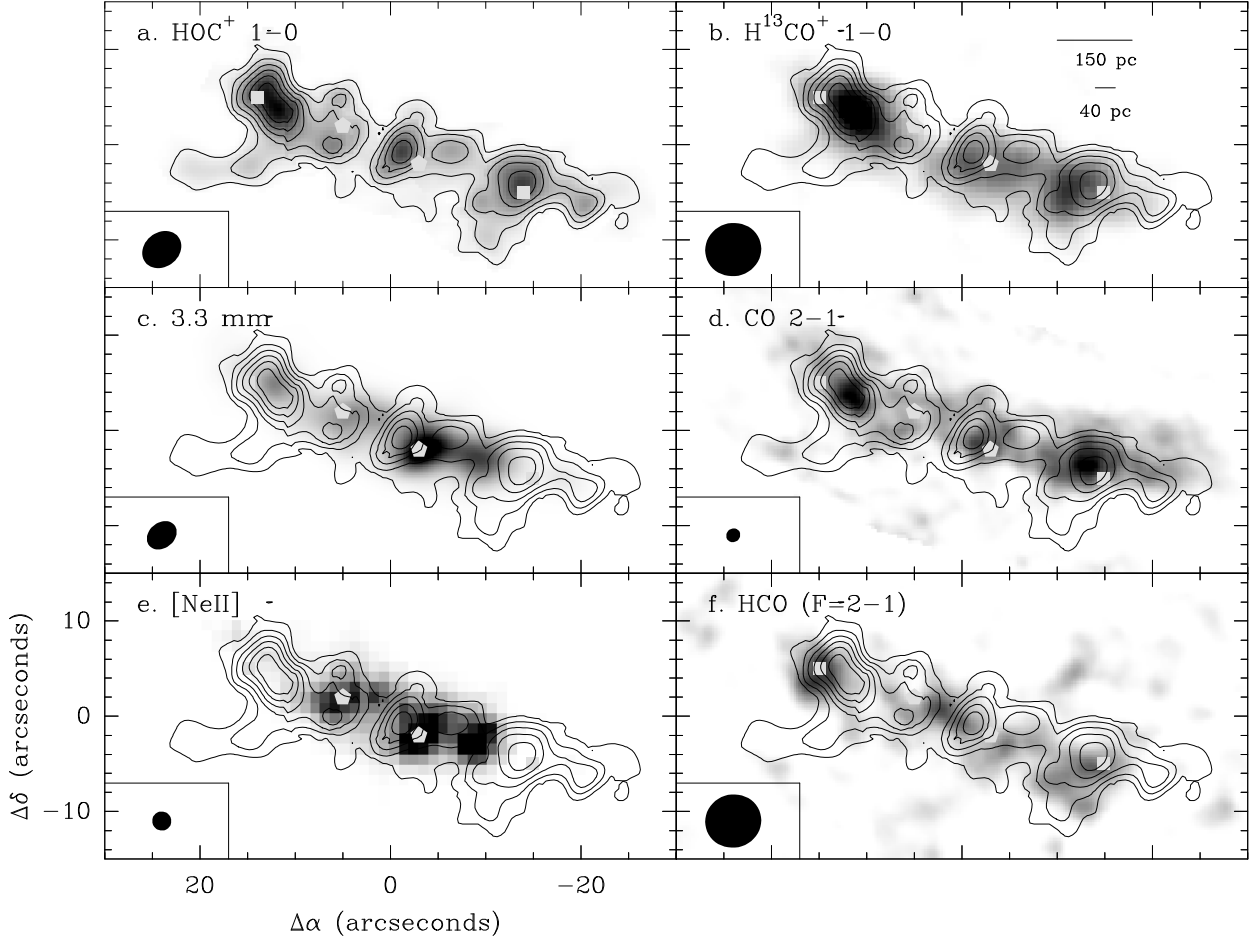


**Fig. 2.** **a.** Integrated intensity image of the HOC<sup>+</sup> 1→0 line as observed with the PdBI interferometer. Contours are 31.8, 77.7, 124.3, 170.9, 217.6 and 264.2 mJy/beam × km/s. The inner ring is indicated by white pentagons and the outer ring by white squares. **b.** The integrated intensity map of the HOC<sup>+</sup> 1→0 line superposed on the interferometric H<sup>13</sup>CO<sup>+</sup> 1→0 image reported in Paper I (grey scale: 100–800 mJy/beam × km/s). **c.** The same as **b.** but on our continuum interferometric image at 3.3mm (grey scale: 1–35 mJy/beam). **d.** The same as **b.** but on the interferometric continuum <sup>12</sup>CO 2→1 image reported by Weiss et al. (2001) (grey scale: 0.7–2.5 Jy/beam × km/s). **e.** The same as **b.** but on the [NeII] image published by Achertman & Lacy (1995) (grey scale: 0.110–0.90 Jy). **f.** The same as **b.** but on the HCO image published in Paper I (grey scale: 100–350 mJy/beam × km/s).

**Table 1.** Line and telescope parameters

| Molecule                        | Transition | Freq. (GHz) | Tel. | HPBW         |
|---------------------------------|------------|-------------|------|--------------|
| H <sup>13</sup> CO <sup>+</sup> | J=1→0      | 86.75433    | PdBI | 5.9''×5.6''  |
| HOC <sup>+</sup>                | J=1→0      | 89.48741    | PdBI | 4.38''×3.6'' |
| HOC <sup>+</sup>                | J=1→0      | 89.48741    | 30m  | 28''         |
| HCO <sup>+</sup>                | J=3→2      | 267.55753   | 30m  | 9''          |
| HOC <sup>+</sup>                | J=3→2      | 268.45109   | 30m  | 9''          |
| HCO <sup>+</sup>                | J=3→2      | 267.55753   | JCMT | 18''         |
| HOC <sup>+</sup>                | J=3→2      | 268.45109   | JCMT | 18''         |
| HCO <sup>+</sup>                | J=4→3      | 356.73413   | JCMT | 14''         |
| HOC <sup>+</sup>                | J=4→3      | 357.92199   | JCMT | 14''         |

To estimate the physical conditions of the emitting gas, mainly the molecular hydrogen density, it is essential to derive accurate values of the (HCO<sup>+</sup> 4→3)/(HCO<sup>+</sup> 3→2) line intensity ( $T_B$ ) ratio (see Sect. 4 and Fig. 4). Since the two lines are observed with different beams, this requires of making some assumptions about the emission spatial distribution. On basis of our H<sup>13</sup>CO<sup>+</sup> 1→0 and HOC<sup>+</sup> 1→0 interferometric images we

have assumed that the emission of the HCO<sup>+</sup> 3→2 and 4→3 lines arises in a uniform slab which is unresolved in the direction perpendicular to the plane. In this case we only need to make a 1-D beam dilution correction to the intensity of the J=4→3 line to get the right line intensity ratio. *With the assumed geometry, the HCO<sup>+</sup> 4→3/HCO<sup>+</sup> 3→2 line intensity ratio is ~0.8 all across the galaxy plane.* We next discuss the quality of our approximation by comparing the intensities of the HCO<sup>+</sup> 3→2 line as measured with the 30m telescope (HPBW~9'') with those measured with the JCMT (HPBW~18'').

The linewidths of the HCO<sup>+</sup> 3→2 line as observed using the 30m and the JCMT telescopes are quite similar towards the E. With our assumption that the emitting region is a uniform slab, the ratio between the line intensities should be ~2. The measured value is 1.4. Taking into account possible relative calibration errors (30%) between the two instruments, our measurements are quite compatible with the assumed geometry.

The linewidths of the HCO<sup>+</sup> 3→2 lines observed with the 30m and the JCMT are, however, very different towards the Center. This is not surprising taking into account that the size of the JCMT beam is twice that of the 30m telescope (see Table 1).

**Table 2.** Gaussian fits to the lines observed with the JCMT

| Transition           | $\int T_{MB} dv$<br>(K km s <sup>-1</sup> ) | $v_{lsr}$<br>(km s <sup>-1</sup> ) | $\Delta v$<br>(km s <sup>-1</sup> ) | $T_{MB}$<br>(mK) |
|----------------------|---|------------------------------------|-------------------------------------|------------------|
| E. (+14",+5")        |   |                                    |                                     |                  |
| HCO <sup>+</sup> 3→2 | 22.6 (0.2)                                  | 296(2)                             | 101(3)                              | 210(11)          |
| HCO <sup>+</sup> 4→3 | 19.9 (0.3)                                  | 305(1)                             | 86(2)                               | 217( 7)          |
| HOC <sup>+</sup> 3→2 | <1 <sup>b</sup>                             |                                    | 101 <sup>a</sup>                    | <33 <sup>b</sup> |
| HOC <sup>+</sup> 4→3 | <0.5  |                                    | 86 <sup>a</sup>                     | <21              |
| Center (0",0")       |   |                                    |                                     |                  |
| HCO <sup>+</sup> 3→2 | 29.4(0.2)                                   | 200(1)                             | 212(2)                              | 130(3)           |
| HCO <sup>+</sup> 4→3 | 17.6(0.3)                                   | 140(2)                             | 122(3)                              | 135(8)           |
| HOC <sup>+</sup> 3→2 | <0.4  |                                    | 212 <sup>a</sup>                    | <9               |
| HOC <sup>+</sup> 4→3 | <0.7  |                                    | 122 <sup>a</sup>                    | <24              |
| W. (-14",-5")        |   |                                    |                                     |                  |
| HCO <sup>+</sup> 3→2 | 16.8(0.3)                                   | 118(1)                             | 90(2)                               | 174(7)           |
| HCO <sup>+</sup> 4→3 | 15.1(0.5)                                   | 111(1)                             | 73(3)                               | 194(17)          |
| HOC <sup>+</sup> 3→2 | <0.6  |                                    | 90 <sup>a</sup>                     | <21              |
| HOC <sup>+</sup> 4→3 | <1.2  |                                    | 73 <sup>a</sup>                     | <51              |

<sup>a</sup> Assumed linewidth to derive the integrated intensity upper limit.

<sup>b</sup> Upper limits are  $3\sigma$ .

Three different velocity components (C1 centered at 255 km/s, C2 at 160 km/s and C3 at 95 km/s) appear in the profile of the HCO<sup>+</sup> 3→2 line as observed with the JCMT (see Fig. 1). Only the component at 160 km/s appears in the 30m spectrum (see Paper III). Assuming again that the emission is uniform in a slab centered in the disk plane and unresolved in the perpendicular direction, one would expect that the intensity measured with the JCMT is a factor of 2 lower than that measured with the 30m because of the different beams. The line intensity of the C2 component is indeed a factor  $\sim 1.7$  lower than the main brightness temperature measured with the IRAM 30m telescope. However this rule does not apply to the integrated intensities because of the contribution of the C1 and C3 components in the JCMT spectrum.

Therefore, we conclude that the assumed geometry is consistent with our 30m and JCMT observations.

### 3.2. Interferometric observations

In Fig. 2 we compare our HOC<sup>+</sup> 1→0 image with the high angular resolution images of M 82 in several molecular lines. Our continuum image at 3.3 mm and the [NeII] map by Achertman & Lacy (1995) are also shown.

All molecular maps depict the typical nested rings morphology, with two maxima located almost symmetrically on both sides of the dynamical center of the galaxy. However, the angular distance between both peaks is different from one species to another. This suggests a chemical stratification of the ring structure. The [Ne II] emission (Achertman & Lacy 1995) and the radio recombination lines (Rodríguez-Rico et al. 2004) define a ring of HII regions with a width of  $\sim 10''$ - $15''$ . The peaks of this ring are marked with pentagons in Fig. 1 and hereafter we will refer to it as the *inner ring*. The CO and H<sup>13</sup>CO<sup>+</sup> maxima lies beyond the HII regions defining a ring with a width of  $\sim 25''$ - $28''$ . The HCO emission extends further out in the disk with a separation of  $\sim 32''$  between the peaks. The peaks of this ring are marked with squares in Fig. 1 and hereafter we will refer to it as *outer ring*. We interpreted this chemical stratification as the consequence of the propagation of the PDR chemistry outwards the disk (Paper I).

The emission of the HOC<sup>+</sup> 1→0 line is weak in the *inner ring*. The HOC<sup>+</sup> emission is concentrated in two maxima lo-

cated at the inner edge of the *outer ring*, at the same distance from the galaxy center as the peaks of the H<sup>13</sup>CO<sup>+</sup> 1→0 and CO 2→1 lines. In fact, the HOC<sup>+</sup> 1→0, H<sup>13</sup>CO<sup>+</sup> 1→0 and CO 2→1 lines have similar spatial distribution at scales of  $\sim 150$  pc. This similarity breaks down at smaller scales, however. The E. maximum of HOC<sup>+</sup> is displaced  $\sim 40$  pc towards the North relative to that of H<sup>13</sup>CO<sup>+</sup>. Similar displacements ( $\sim 40$  pc) between the HOC<sup>+</sup> and H<sup>13</sup>CO<sup>+</sup> maxima are observed at several positions in the western-half of the M 82 disk. The spatial distributions of the CO 2→1 and HOC<sup>+</sup> 1→0 lines are quite different in the region enclosed by the *inner ring*. This is very likely due to the different critical densities of the two transitions. Mao et al. (2000) claimed that the bulk of the CO emission is arising in a warm low density interclump medium instead of in the dense clouds. The spatial distribution of the HOC<sup>+</sup> 1→0 line is certainly very different from that of the HCO F=2→1 line. The HOC<sup>+</sup> emission is displaced, in z-direction, towards the North and, in radial direction, towards the center of the galaxy relative to that of HCO. A very different spatial distribution between HCO and the other PDR tracers H<sup>13</sup>CO<sup>+</sup>, HOC<sup>+</sup>, and CO<sup>+</sup>, is also observed in the Galactic PDR associated to the ultracompact HII region Mon R2 (Rizzo et al. 2003, 2005).

#### 3.2.1. H<sup>13</sup>CO<sup>+</sup>/HOC<sup>+</sup>

To quantify the observed differences between the spatial distribution of the H<sup>13</sup>CO<sup>+</sup> 1→0 and HOC<sup>+</sup> 1→0 lines, we have calculated the map of the H<sup>13</sup>CO<sup>+</sup> 1→0/HOC<sup>+</sup> 1→0 brightness temperature ratio (hereafter,  $R$ ) using our PdBI images convolved to the same angular resolution ( $5.9'' \times 5.6''$ ). The resulting image is shown in Fig. 2.  $R$  takes values between 1 and 2 in most of the galaxy disk without any clear trend with the distance from the galaxy center. This is consistent with the uniform value of  $R$  measured with the 30m telescope (Paper II). Larger values,  $R \geq 3$ , are found in the southern half of the bubble associated with the supernova remnant SNR 41.95+57.5, which produces a North-South gradient in the value of  $R$  towards the western-half of the M 82 disk. Since the excitation conditions of the H<sup>13</sup>CO<sup>+</sup> 1→0 and HOC<sup>+</sup> 1→0 lines are quite similar, this displacement is very likely due to a gradient in the [H<sup>13</sup>CO<sup>+</sup>]/[HOC<sup>+</sup>] abundance ratio. Assuming a <sup>12</sup>CO/<sup>13</sup>CO ratio of 89 and the two isotopomers arising in the same phase, values of  $R$  between  $\sim 1$  and  $\sim 3$  corresponds to [HCO<sup>+</sup>]/[HOC<sup>+</sup>] between  $\sim 44$  and  $\sim 136$ . These values are similar to those found in Galactic PDRs (Fuente et al. 2003, Rizzo et al. 2003, Savage & Ziurys 2004) and towards the AGN in NGC 1068 (Usero et al. 2004) but more than one order of magnitude larger than those found in Galactic dense clouds where [HCO<sup>+</sup>]/[HOC<sup>+</sup>]=2000–6000 (Apponi & Ziurys 1997).

## 4. LVG calculations

We have made LVG calculations to derive the physical conditions of the emitting gas. Chemical models show that high electron abundances,  $X(e^-) > 10^{-5}$ , are required to have such low values of the [HCO<sup>+</sup>]/[HOC<sup>+</sup>] ratio,  $< 80$ , as measured in M 82 (see Paper II, Usero et al. 2004, Fuente et al. 2003). Therefore, part of the HCO<sup>+</sup> and most HOC<sup>+</sup> emission is very likely arising in the partially ionized cloud envelopes and/or intercloud medium, and collisions with electrons should be considered in our molecular excitation calculations. We have calculated the HCO<sup>+</sup> and HOC<sup>+</sup> collisional rates with electrons using the method described in Appendix A. While collisional rates with molecular hydrogen

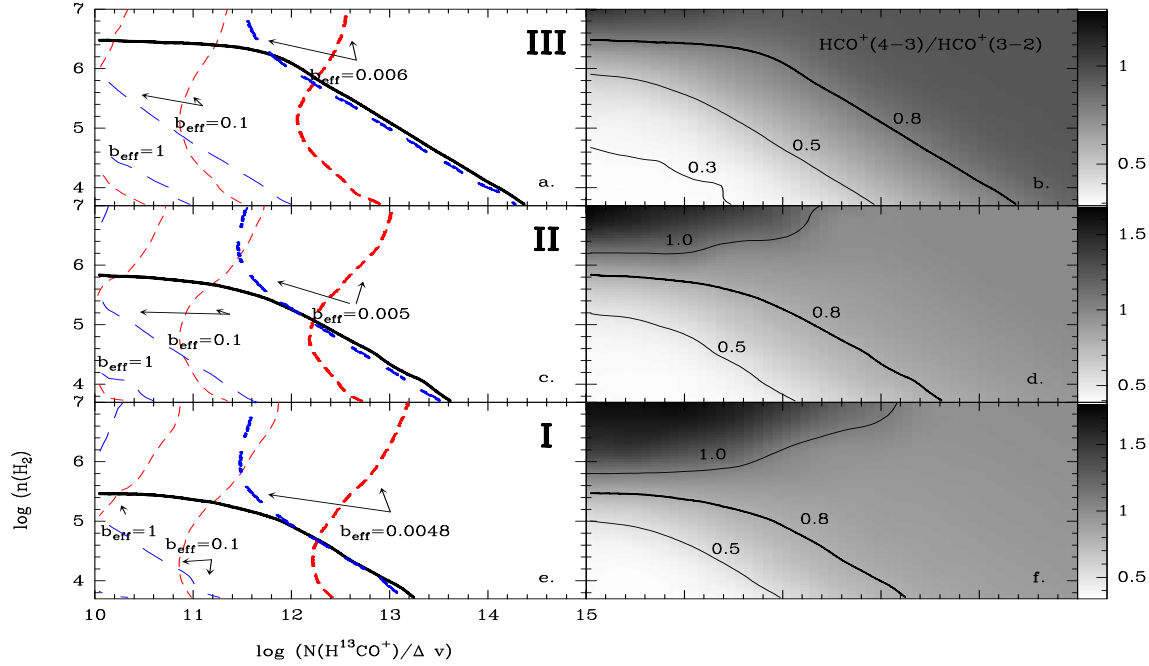


**Fig. 4.** Results from our LVG calculations assuming typical physical conditions of the regions III (top), II (middle) and I (bottom) of the PDR (see Fig. 6 and text). In the right panels (b., d. and f.) we show the HCO<sup>+</sup> 4→3/HCO<sup>+</sup> 3→2 line ratio as a function of the hydrogen density ( $n(\text{H}_2)$ ) and the HCO<sup>+</sup> column density,  $N(\text{HCO}^+) = 89 \times N(\text{H}^{13}\text{CO}^+)$ . Left panels (a., c. and e.) have to be interpreted as follows: the continuous line is the contour corresponding to a HCO<sup>+</sup> 4→3/HCO<sup>+</sup> 3→2 line intensity ratio of 0.8. The HCO<sup>+</sup> 4→3/HCO<sup>+</sup> 3→2 line intensity ratio does not depend on the beam filling factor because we assume that it is the same for the two lines. Short-dashed lines correspond to an observed H<sup>13</sup>CO<sup>+</sup> 1→0 intensity of 9.1 mK (value observed towards the E.) assuming different values of the beam filling factor for this line emission. Long-dashed lines are the contours for a HCO<sup>+</sup> 3→2 intensity of 210 mK (value toward the E.) assuming a  $[\text{HCO}^+]/[\text{H}^{13}\text{CO}^+] = 89$  and the same values of the beam filling factor as for the H<sup>13</sup>CO<sup>+</sup> line. Note that we only find a solution for a beam filling factor of 0.006 in region III, 0.005 assuming in region II and of 0.0048 in region I. These are the solutions given in Table 3.

are of the order of  $10^{-10} \text{ cm}^{-3} \text{ s}^{-1}$ , the collisional rates with electrons are  $\sim 10^{-5} \text{ cm}^{-3} \text{ s}^{-1}$ , which corroborates that collisions with electrons are to be considered in our case (in which  $X(e^-) > 10^{-5}$ ).

We have derived the physical conditions of the gas emitting in HCO<sup>+</sup> by fitting the spectra derived from the H<sup>13</sup>CO<sup>+</sup> image smoothed to a beam of 18", and the JCMT observations. In our LVG analysis we have assumed a constant  $[\text{HCO}^+]/[\text{H}^{13}\text{CO}^+]$  isotopic ratio of 89 and considered three different sets of kinetic temperature/electron density values that defined the typical stratification within a cloud irradiated by an intense UV field: (I)  $T_k = 1000 \text{ K}$ ,  $X(e^-) = 10^{-3}$ ; (II)  $T_k = 200 \text{ K}$ ,  $X(e^-) = 10^{-4}$ ; and (III)  $T_k = 50 \text{ K}$ ,  $X(e^-) = 0$ . These three regions are shown in Fig. 6 for a plane-parallel slab with a total visual extinction of 50 mag with the two sides illuminated by the intense UV field prevailing in M 82.

In regions II and III the hydrogen is mainly in molecular form and collisions with H<sub>2</sub> dominates the excitation of the HCO<sup>+</sup> molecules. However, more than 50% (the exact value depends on the exact value of the visual extinction) of the hydrogen is in atomic form in region I. Collisions with H could dominate in this region because the rates for H are usually larger than those for H<sub>2</sub> (partly because H is lighter than H<sub>2</sub>). As the rates for H are not known for this ion, we can consider that the present para-H<sub>2</sub> rates (Flower, 1999) can be used for H atoms within a factor of 5. Such difference between H and H<sub>2</sub> collisions rates are in-

deed observed for CO (Flower 2001, Balakrishnan et al, 2002). Thus our final estimate of the molecular hydrogen density in region I is actually a particle (H and H<sub>2</sub>) density and is accurate within a factor of 5.

The results of our excitation calculations are shown in Table 3. Since we have observed two lines of the main isotope HCO<sup>+</sup>, and one of the rarer isotope, H<sup>13</sup>CO<sup>+</sup>, we can determine the opacity of the lines and derive the beam filling factor, the H<sup>13</sup>CO<sup>+</sup> (and therefore HCO<sup>+</sup>) column density and the molecular hydrogen density from our LVG fitting. Our observations are well accounted for by beam filling factors between 0.003-0.006, which at the distance of M 82 correspond to typical sizes of 20–30 pc, similar to the size of a giant molecular cloud in our Galaxy. Note, however, that this is an area beam filling factor and the linear size derived in this way is only an upper limit to the actual cloud sizes. The H<sup>13</sup>CO<sup>+</sup> column density is  $N(\text{H}^{13}\text{CO}^+)/\Delta v \sim 2 \cdot 10^{12} \text{ cm}^{-2}$  towards the three positions. This value is quite robust since it is not strongly dependent on the assumed values of the kinetic temperature and electron abundance (see Fig. 4). The derived values of  $n(\text{H}_2)$  do, however, depend on the assumed kinetic temperature and electron abundance. For negligible values of  $X(e^-)$  we obtain molecular hydrogen densities larger than  $5 \times 10^5 \text{ cm}^{-3}$ . The derived value of the molecular hydrogen density is lower by an order of magnitude if a kinetic temperature of 1000 K and an electron abundance of  $10^{-3}$  are assumed (see Table 3 and Fig. 4). The derived molecular hydrogen

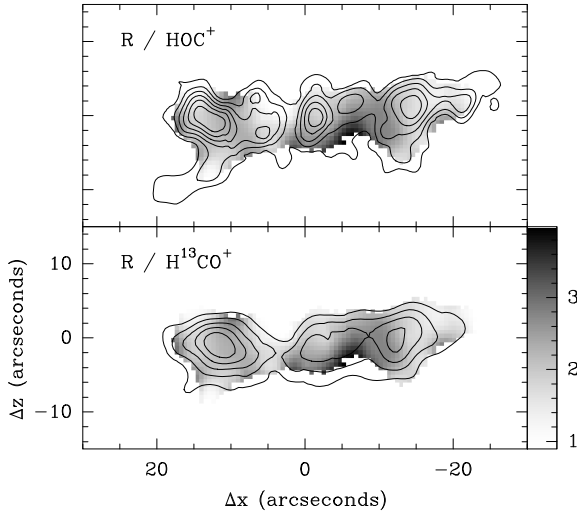


**Fig. 3.** Map of the H<sup>13</sup>CO<sup>+</sup> 1→0/HOC<sup>+</sup> 1→0 brightness temperature ratio, R, (grey scale) in M 82. The galaxy has been rotated to make coincide its major axis with the abscissas axis. In the top panel we compare the H<sup>13</sup>CO<sup>+</sup> 1→0/HOC<sup>+</sup> 1→0 image with that of the integrated intensity emission of the HOC<sup>+</sup> 1→0 line, in the bottom, with that of H<sup>13</sup>CO<sup>+</sup> 1→0 line (Paper I).

**Table 3.** LVG results

|        | X(e <sup>-</sup> ) | b <sub>eff</sub> | N(H <sup>13</sup> CO <sup>+</sup> )/Δv<br>(cm <sup>-2</sup> km <sup>-1</sup> s) | n(H <sub>2</sub> )<br>(cm <sup>-3</sup> ) | T <sub>k</sub><br>(K) |
|--------|--------------------|------------------|---|---|-----------------------|
| E.     | 0                  | 0.006            | 1.9 10 <sup>12</sup>  | 6.0 10 <sup>5</sup>                       | 50                    |
| Center | 0                  | 0.0035           | 1.5 10 <sup>12</sup>  | 7.4 10 <sup>5</sup>                       | 50                    |
| W.     | 0                  | 0.0048           | 2.3 10 <sup>12</sup>  | 5.5 10 <sup>5</sup>                       | 50                    |
| E.     | 10 <sup>-4</sup>   | 0.005            | 1.7 10 <sup>12</sup>  | 1.1 10 <sup>5</sup>                       | 200                   |
| Center | 10 <sup>-4</sup>   | 0.003            | 1.2 10 <sup>12</sup>  | 1.5 10 <sup>5</sup>                       | 200                   |
| W.     | 10 <sup>-4</sup>   | 0.004            | 2.2 10 <sup>12</sup>  | 9.2 10 <sup>4</sup>                       | 200                   |
| E.     | 10 <sup>-3</sup>   | 0.0048           | 1.7 10 <sup>12</sup>  | 5.0 10 <sup>4</sup>                       | 1000                  |
| Center | 10 <sup>-3</sup>   | 0.0042           | 1.3 10 <sup>12</sup>  | 6.8 10 <sup>4</sup>                       | 1000                  |
| W.     | 10 <sup>-3</sup>   | 0.006            | 2.3 10 <sup>12</sup>  | 4.0 10 <sup>4</sup>                       | 1000                  |

densities are larger than 10<sup>4</sup> cm<sup>-3</sup> even in the case of the extreme physical conditions of region I. This proves that the bulk of the HCO<sup>+</sup> emission is arising from dense gas.

For HOC<sup>+</sup> our information is not complete. We have detected the HOC<sup>+</sup> 3→2 line towards the E. using the 30m telescope (Paper III). We have not detected the HOC<sup>+</sup> 3→2 line towards any position using the JCMT. Using the 30m data and our interferometric HOC<sup>+</sup> J=1→0 image degraded to an angular resolution of 9'', we have made some LVG calculations and estimated the physical conditions of the gas emitting in HOC<sup>+</sup>. Assuming T<sub>k</sub>=50 K and X(e<sup>-</sup>)=0, we derive a beam averaged HOC<sup>+</sup> column density, N(HOC<sup>+</sup>)/Δv=2.8 10<sup>12</sup> cm<sup>-2</sup>, and a molecular hydrogen density, n(H<sub>2</sub>)~1 10<sup>5</sup> cm<sup>-3</sup>, towards the E. The derived molecular hydrogen density is only a few times lower than that derived from the HCO<sup>+</sup> lines assuming the same physical conditions. As discussed in Section 5, these physical conditions are not realistic for HOC<sup>+</sup> that is expected to mainly arise in region I. Assuming the most extreme physical conditions of region I, T<sub>k</sub>=1000 K and X(e<sup>-</sup>)=10<sup>-3</sup>, the derived H<sub>2</sub> density is ~ 2 10<sup>4</sup> cm<sup>-3</sup>. This large density (>10<sup>4</sup> cm<sup>-3</sup>) suggests that the

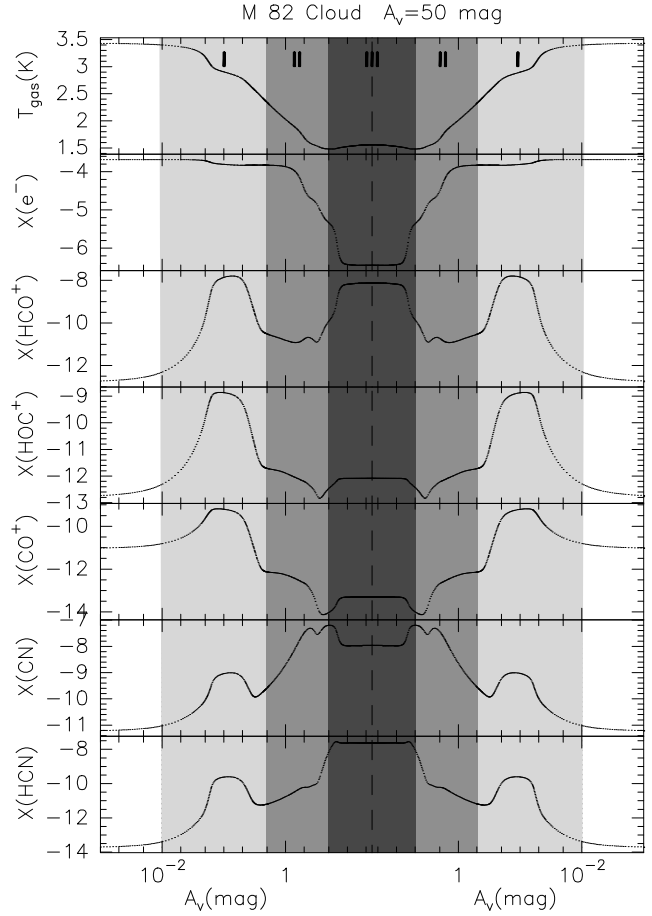


**Fig. 6.** Predictions for the gas temperature, electronic abundance and abundances of various species derived with our improved PDR model. The calculations have been carried out for a plane-parallel cloud of 50 mag, with a uniform density of  $n = 4 \cdot 10^5 \text{ cm}^{-3}$ , that is being illuminated by a UV field of  $G_0 = 1.0 \cdot 10^4$  (in units of the Habing field) from the two sides. The cosmic rays flux is set to  $\zeta = 4 \cdot 10^{-15} \text{ s}^{-1}$ . We have shadowed the three regions discussed in Section 4 and 5.

HOC<sup>+</sup> emission arises in the partially ionized cloud envelopes rather than in the diffuse intercloud medium proposed by Mao et al. (2000) to explain the CO observations.

## 5. Discussion

Following we discuss the two scenarios proposed to explain the large reactive ions abundances in M 82, UV-photon and X-ray dominated chemistry, on basis of our new observational results and model calculations.

### 5.1. Is X-ray chemistry at work in M 82?

Spaans and Meijerink (2007) proposed that the diffuse X-ray emission at 0.7 keV could contribute to produce the high abundances of reactive ions measured towards M 82. To have a deeper insight into the chemistry of these ions, we have compared our high-angular resolution HOC<sup>+</sup> image with the spatial distribution of the X-ray emission.

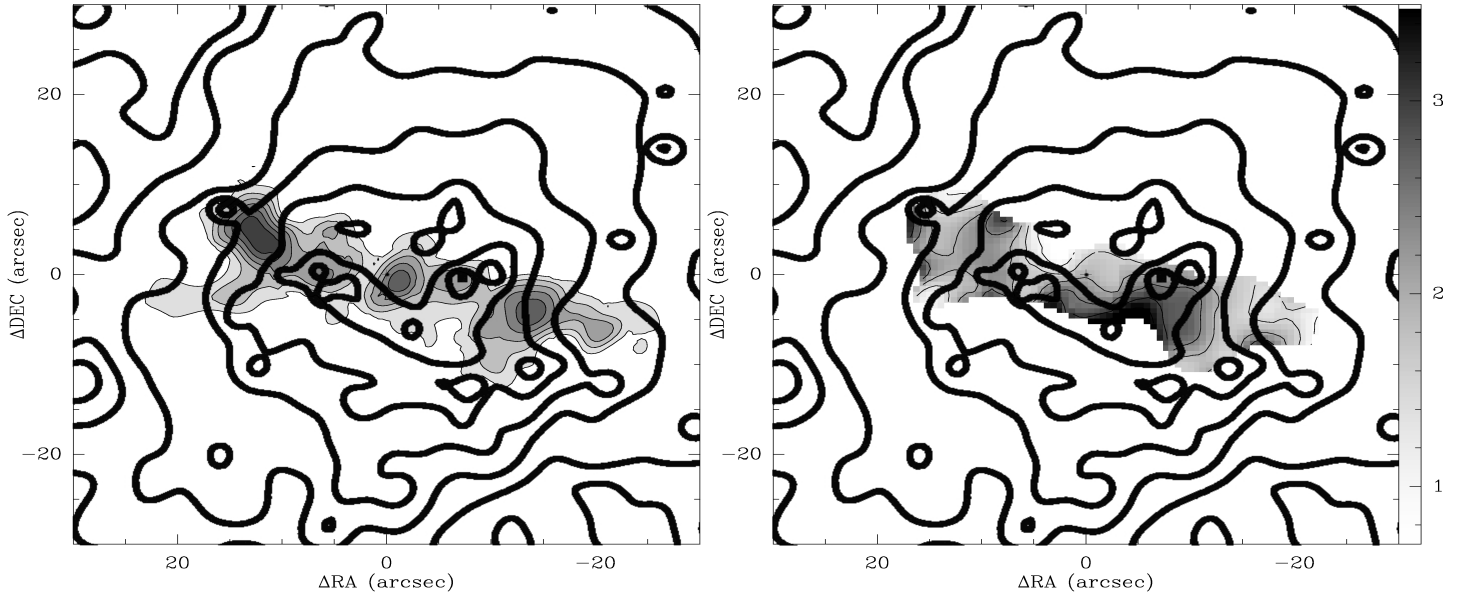


**Fig. 5.** Comparison between the spatial distribution of the diffuse hard X-ray emission (1.6-2.2 keV) with that of the HOC<sup>+</sup> emission (**left panel**) and the (H<sup>13</sup>CO<sup>+</sup> 1→0)/(HOC<sup>+</sup> 1→0) brightness temperature ratio (**right panel**). Note the HOC<sup>+</sup> emission is not spatially correlated with the diffuse hard X-ray emission nor the (H<sup>13</sup>CO<sup>+</sup> 1→0)/(HOC<sup>+</sup> 1→0) brightness temperature ratio. (The X-ray image has been taken from Strickland & Heckman 2007).

Strickland and Heckman (2007) reported the images of the continuum diffuse X-ray emission in the central 2 kpc × 2 kpc of M 82 for the energy bands between 0.3 to 7.0 KeV. The diffuse, both soft and hard, X-ray emission arises from the inner ~350 pc (20'') of the galaxy and extends along the outflow lobes. The soft X-ray emission (E < 1.1 keV) is heavily absorbed by the material in the galaxy plane and peaks in the outflow lobes (at z > 20''). In contrast, the less absorbed diffuse hard X-ray emission (E < 1.1 keV) is intense in the galaxy disk and extends only ~8'' and ~12'' above and below the galaxy plane.

Since soft X-rays are heavily extinguished towards the galaxy plane, a detailed comparison between the spatial distribution of the soft X-ray flux and the HOC<sup>+</sup> emission is not possible. However, it is clear from the X-ray images that the soft X-rays are associated with the superwind itself and the superwind sources. The superwind is generated in the inner 350 pc of the galaxy where intense diffuse hard X-ray emission is detected.

In Fig. 5 we superpose the image of the diffuse hard X-rays emission in the band 2.2-2.8 keV published by Strickland and Heckman (2007) on our HOC<sup>+</sup> and the [H<sup>13</sup>CO<sup>+</sup>]/[HOC<sup>+</sup>] images. Within the disk plane, the X-ray emission is concentrated in the region enclosed by the *inner ring* where only weak HOC<sup>+</sup> emission is found. In fact the two most intense HOC<sup>+</sup> maxima are located just outside the X-rays emitting region. Even towards the center of the galaxy, the most intense HOC<sup>+</sup> peak seems to avoid the peaks of the X-ray emission.

There is no obvious relationship between the values of the [H<sup>13</sup>CO<sup>+</sup>]/[HOC<sup>+</sup>] ratio and the diffuse hard X-ray emission, either. Unlike the X-ray emission, the [H<sup>13</sup>CO<sup>+</sup>]/[HOC<sup>+</sup>] ratio does not present any systematic trend with the distance from the galaxy center. Moreover, the [H<sup>13</sup>CO<sup>+</sup>]/[HOC<sup>+</sup>] ratio presents the highest value around SNR 41.95±57.5, the most intense X-ray source of the galaxy. Therefore, morphological arguments do

not support the scenario of X-rays being the driving agent of the reactive ions chemistry in M 82.

An independent argument against the XDR scenario comes from the different spatial distribution of the HOC<sup>+</sup> and SiO emissions in M 82. Usero et al. (2004) detected large SiO and HOC<sup>+</sup> abundances towards the circumnuclear region (CND) in NGC 1068. In this case, the large SiO and HOC<sup>+</sup> abundances were interpreted in terms of the interactions between the X-rays and, respectively, the dust and gas in the CND. Unlike NGC 1068, the SiO and the HOC<sup>+</sup> emissions arise in different regions towards M 82. While the HOC<sup>+</sup> emission arises in the galaxy disk (this Paper), the SiO emission is tracing the gas outflowing from the galaxy plane (García-Burillo et al. 2001). This different spatial distribution suggest a different origin for the HOC<sup>+</sup> and SiO emission in M 82 from that in NGC 1068.

## 5.2. PDR model

In this section, we explore the possibility of explaining the molecular abundances observed in M 82 in terms of PDR chemistry. For this aim, we have used the updated version of the Meudon PDR code (Le Petit et al. 2006). The chemical network has been enlarged, relative to Paper III, to include the chemistry of HOC<sup>+</sup>. Some reactions rates have also been updated according to the Ohio State University database (<http://www.physics.ohio-state.edu/~eric/>). In particular, the reaction rate of C<sup>+</sup> + OH → CO<sup>+</sup> + H has been increased to 2.9 10<sup>-9</sup> cm<sup>-3</sup> s<sup>-1</sup>, which translates into a larger CO<sup>+</sup> production and a better agreement between our predictions and the observational results as we will discuss below. We have also included a new CO<sup>+</sup> formation reaction, O + CH<sup>+</sup> → CO<sup>+</sup> + H, but its contribution to the total CO<sup>+</sup> formation is very low (<3%).

In Paper III, we fitted the  $[\text{CO}^+]/[\text{HCO}^+]$ ,  $[\text{HCO}^+]/[\text{HOC}^+]$  and  $[\text{CN}]/[\text{HCN}]$  ratios with a plane-parallel model, assuming  $G_0=10^4$  in units of the Habing field,  $n=4 \cdot 10^5 \text{ cm}^{-3}$ , a cosmic ray flux of  $4 \cdot 10^{-15} \text{ s}^{-1}$  and clouds with a total thickness of  $\sim 13 \text{ mag}$ . The thickness of the clouds was estimated as twice the thickness of the plane-parallel one side illuminated PDR that fits the observations. Our model was quite successful in predicting the  $[\text{CO}^+]/[\text{HCO}^+]$ ,  $[\text{HCO}^+]/[\text{HOC}^+]$  and  $[\text{CN}]/[\text{HCN}]$  abundance ratios but could not account for the measured  $\text{CO}^+$  column densities. We needed about  $\sim 20\text{--}40$  clouds along the line of sight to explain the CN column densities, but then the predicted  $\text{CO}^+$  column densities fell short by one order of magnitude. Conversely, if we fitted the  $\text{CO}^+$  column densities, the predicted CN column densities were far in excess. This option looked less plausible because of the large number of clouds required to fit the  $\text{CO}^+$  column densities ( $>100$ ).

With our new chemical network, we obtain  $\text{CO}^+$  column densities a factor of  $\sim 5$  larger than before (see Table 5). To improve our model, we have assumed, in addition, a plane-parallel cloud illuminated from the two sides. This is a more realistic view of the ISM in M 82. The parameters of our PDR model are shown in Table 4.

In Fig. 6 we show our model predictions for a plane-parallel cloud with a total visual extinction of 50 mag. The physical and chemical conditions are symmetric since the cloud is illuminated from the two sides by the same UV field. We can distinguish three regions across the cloud according to their chemical properties: **(I)**  $A_v=0.01\text{--}0.5 \text{ mag}$  from the cloud surface.  $\text{CO}^+$ ,  $\text{HCO}^+$ ,  $\text{HOC}^+$ , CN and HCN present an abundance peak in this region and  $[\text{CN}]/[\text{HCN}]\sim 20$ . **(II)**  $A_v=0.5\text{--}5 \text{ mag}$  from the cloud surface. The abundances of  $\text{CO}^+$ ,  $\text{HCO}^+$ ,  $\text{HOC}^+$  decline in this region. CN and HCN are, however, very abundant and  $[\text{CN}]/[\text{HCN}]\sim 100$ . **(III)**  $A_v>5 \text{ mag}$  from the cloud surface. The reactive ions  $\text{CO}^+$  and  $\text{HOC}^+$  have negligible abundances but  $\text{HCO}^+$ , CN and HCN are abundant with  $[\text{CN}]/[\text{HCN}]\sim 1$ . Note that the reactive ions  $\text{CO}^+$  and  $\text{HOC}^+$  only survive in region I. Therefore, reactive ions are excellent tracers of the number of clouds since their total column density remains constant regardless of the thickness of the cloud for clouds with  $A_v>2 \text{ mag}$ .

In Tables 5, 6 and 7, we compare the predicted molecular column densities and abundance ratios with those observed towards M 82. In addition to  $\text{CO}^+$ ,  $\text{HOC}^+$ ,  $\text{HCO}^+$ , CN, HCN and HCO, we include the  $\text{H}_3\text{O}^+$  column density derived by van der Tak et al. (2008) and the upper limit to the  $\text{H}_2\text{O}$  column density obtained by Wilson et al. (2007). Thus, the most relevant molecules for the PDR/XDR chemistry are considered.

In Table 6 we show a comparison between our one-type-cloud model and the column densities measured towards the E. position in M 82 (Paper I, II, III; van der Tak et al. 2008). This is the position towards which the emission of most molecules peak and column densities are better determined. The number of clouds along the line of sight have been calculated using the  $\text{HOC}^+$  column densities. To match the observed  $\text{HOC}^+$  column density, we use 44 clouds of  $A_v=5$ . This choice provides a good fit (within a factor of 3) to many of the other observed column densities (see Table 7). However, the model falls short by 2 orders of magnitude to predict the HCN column densities. Related to it, the  $[\text{CN}]/[\text{HCN}]$  ratio is  $\sim 380$ , far in excess the observed value. The model does not reproduce the HCO and  $\text{H}_2\text{O}$  column densities either. Moving to  $\sim 10 \text{ mag}$  clouds, we need 40 clouds along the line of sight to fit the  $\text{HOC}^+$  column density. In this case, we improve our fit to the HCN column density and the  $[\text{CN}]/[\text{HCN}]$  ratio, but the predicted CN and  $\text{H}_3\text{O}^+$  column densities are then too large. This is the same problem we found in

Paper III. We cannot fit the CN, HCN, and reactive ions column densities simultaneously. The new reaction rates improve the fit but not enough. The fit would become worse if we go to larger clouds. The  $[\text{CN}]/[\text{HCN}]$  ratio would decrease and get closer to the observed value but the predicted CN, HCN,  $\text{HCO}^+$  and  $\text{H}_3\text{O}^+$  column densities would increase and become much larger than the observed values.

In order to look for a better solution, we have tried a two-cloud-type model. We obtain a good agreement with the observations by assuming that we have  $\sim 44$  clouds, 98.5% of which have a thickness  $\sim 5 \text{ mag}$  but a few percentage, 1.5%, have a thickness of 50 mag. Since the assumed cloud morphology (a column plane-parallel cloud) is not realistic, the number of clouds has here only a statistical meaning. It means that the emission can be explained with a cloud distribution such that most of the molecular gas (87%) is forming small clouds (represented by our plane-parallel  $A_v=5 \text{ mag}$  cloud) while only a few percentage (13%) is in larger molecular clouds (represented by our plane-parallel  $A_v=50 \text{ mag}$  cloud). Compared with the case of 100% of small clouds, the small percentage of large clouds inject the lacking HCN column density and push down the CN/HCN ratio to fit the observed value of  $\sim 6$  without changing that much the  $[\text{CO}^+]/[\text{HCO}^+]$  and  $[\text{HCO}^+]/[\text{HOC}^+]$  ratios. In addition, our predicted HCO column densities are much closer, although still below, the observed value. Note that the number of large clouds is limited by the HCN and  $\text{HCO}^+$  column densities. Both species are very abundant in region III of our pattern 50 mag cloud and their column densities increase rapidly with the number of large clouds. With the proposed mix, we fit all the observed column densities except those of HCO and  $\text{H}_2\text{O}$ .

Our model falls short by a factor of 10 to predict the observed HCO column densities. Schilke et al. (1992) proposed that the photodissociation of the  $\text{H}_2\text{CO}$  molecules released from the grain mantles could increase the HCO abundance in the moderately illuminated regions of the PDR. Our model does not include production of these species on grains.

Regarding  $\text{H}_2\text{O}$ , the predicted column densities are 2 orders of magnitude larger than the upper limit obtained by Wilson et al. (2007). This discrepancy is very likely because we are using a gas-phase model that neglects the depletion of water in dense clouds. It is also important to recall that this limit was obtained with a large beam ( $2.1''$ ) and by observing the 556.936 GHz transition of ortho- $\text{H}_2\text{O}$  which is very likely optically thick. Therefore, the limit is quite uncertain.

Summarizing, we conclude that the most relevant PDR molecules are well fitted by assuming that most of the mass of the molecular gas (87%) is forming small clouds with a total thickness of  $\sim 5 \text{ mag}$ . A small percentage, however, is encompassed in large molecular clouds,  $\sim 50 \text{ mag}$ , in which star formation might be proceeding. This suggests that the mass distribution of the clouds in M 82 is very different from that in our Galaxy, and most of the giant molecular clouds (GMCs) have already been destroyed by the recent starburst. M 82 is, therefore, an old starburst where star formation has almost exhausted the molecular gas reservoir.

## 6. Conclusions

In this paper, we present new JCMT observations of the  $\text{HCO}^+$  and  $\text{HOC}^+$   $3\rightarrow 2$  and  $4\rightarrow 3$  lines and the PdB interferometric image of the  $\text{HOC}^+$   $1\rightarrow 0$  line towards the nucleus of M 82. Our results can be summarized as follows:

**Table 4.** PDR model

|                            |                      |
|----------------------------|----------------------|
| $G_0$ (Habing)             | $1 \cdot 10^4$       |
| $n$ (cm <sup>-3</sup> )    | $4 \cdot 10^5$       |
| $\zeta$ (s <sup>-1</sup> ) | $4 \cdot 10^{-15}$   |
| He                         | 0.1                  |
| C                          | $1.32 \cdot 10^{-4}$ |
| O                          | $3.19 \cdot 10^{-4}$ |
| N                          | $7.50 \cdot 10^{-5}$ |
| S                          | $1.86 \cdot 10^{-5}$ |
| Fe                         | $1.50 \cdot 10^{-8}$ |

**Table 5.** Model Results (I)

| $A_v$<br>(mag) | $\frac{CN}{HCN}$ | $\frac{HCO^+}{HOC^+}$ | $\frac{CO^+}{HCO^+}$ | $\frac{CN}{CO^+}$ |
|----------------|------------------|-----------------------|----------------------|-------------------|
| M 82           | 6                | 44                    | 0.04                 | 420               |
| 2              | 18               | 12                    | 0.04                 | 7                 |
| 5              | 380              | 12                    | 0.04                 | 479               |
| 10             | 38               | 13                    | 0.04                 | 2129              |
| 30             | 1.3              | 305                   | 0.002                | 4193              |
| 50             | 0.9              | 671                   | $7 \cdot 10^{-4}$    | 5397              |
| 100            | 0.6              | 1500                  | $3 \cdot 10^{-4}$    | 8519              |

- We have carried out excitation calculations for HCO<sup>+</sup> and HOC<sup>+</sup> taking into account our 30m and JCMT observations of the HCO<sup>+</sup> and HOC<sup>+</sup> J=3→2 and J=4→3 lines. Our results show that the two ions arise in dense gas ( $n > 10^4$  cm<sup>-3</sup>). Therefore, HOC<sup>+</sup> is likely tracing the partly ionized and moderately dense envelopes of molecular clumps, rather than in the intercloud medium or wind phase.
- We present a high angular resolution (4'') image of HOC<sup>+</sup> 1→0 in M 82, the first ever obtained in Galactic and extragalactic research. The comparison between the diffuse X-ray emission and our HOC<sup>+</sup> image discards X-rays as the major driver of the high abundances of reactive ions in M 82. UV photons from massive stars seem, therefore, the major drivers of the molecular chemistry in M 82.
- Our PDR chemical model shows that most molecular abundances measured towards M 82 (HCO<sup>+</sup>, HOC<sup>+</sup>, CO<sup>+</sup>, CN, HCN, H<sub>3</sub>O<sup>+</sup>) are well accounted in the scenario of two-types (different thickness,  $A_v=5$  mag and  $A_v=50$  mag) of dense clouds ( $> 10^4$  cm<sup>-3</sup>) bathed by an intense interstellar UV field ( $G_0=10^4$ ).
- Furthermore, our model shows that most of the molecular gas, 87 % in mass, is forming small clouds ( $A_v \sim 5$  mag) while only 13% is in large molecular clouds ( $A_v \sim 50$  mag). This suggests that only a small percentage (<13%) of the molecular gas in M 82 is regions where massive star formation is still proceeding.

*Acknowledgements.* We thank the IRAM and JCMT staff for their help and support during the observations and data reduction. AU has been supported through a Post Doctoral Research Assistantship from the UK Science & Technology Facilities Council. We are also grateful to C. Joblin, O. Berné and J.R. Goicoechea for fruitful discussions on the PDR chemistry.

## References

Achtermann, J. M., & Lacy, J. H. 1995, ApJ, 439, 163  
 Apponi, A. J., & Ziurys, L. M. 1997, ApJ, 481, 800  
 Balakrishnan, N., Yan, M., & Dalgarno, A. 2002, ApJ, 568, 443  
 Defrees, D. J., Loew, G. H., McLean, A. D., 1982, ApJ, 257, 376  
 Faure, A., Tennyson, J., 2001, MNRAS, 325, 443  
 Faure, A., Gorfinkel, J. D., Tennyson, J., 2004, MNRAS, 347, 323

Faure, A., Kokoouline, V., Greene, C. H., Tennyson, J., 2006, J. Phys. B, 39, 4261  
 Flower, D. R., 1999, MNRAS, 305, 651  
 Flower, D. R. 2001, Journal of Physics B Atomic Molecular Physics, 34, 2731  
 Fuente, A., Black, J. H., Martín-Pintado, J., Rodríguez-Franco, A., García-Burillo, S., Planesas, P., & Lindholm, J. 2000, ApJ, 545, L113  
 Fuente, A., Rodríguez-Franco, A., García-Burillo, S., Martín-Pintado, J., & Black, J. H. 2003, A&A, 406, 899  
 Fuente, A., García-Burillo, S., Gerin, M., Teyssier, D., Usero, A., Rizzo, J. R., & de Vicente, P. 2005, ApJL, 619, L155 (Paper II)  
 Fuente, A., García-Burillo, S., Gerin, M., Rizzo, J. R., Usero, A., Teyssier, D., Roueff, E., & Le Bourlot, J. 2006, ApJL, 641, L105 (Paper III)  
 García-Burillo, S., Martín-Pintado, J., Fuente, A., & Neri, R. 2001, ApJ, 563, L27  
 García-Burillo, S., Martín-Pintado, J., Fuente, A., Usero, A., & Neri, R. 2002, ApJL, 575, L55 (Paper I)  
 Jiménez-Serra, I., Martín-Pintado, J., Viti, S., Martín, S., Rodríguez-Franco, A., Faure, A., Tennyson, J., 2006, ApJ, 650, L135  
 Le Petit, F., Nehm, C., Le Bourlot, J., & Roueff, E. 2006, ApJS, 164, 506  
 Lord, S. D., Hollenbach, D. J., Haas, M. R., Rubin, R. H., Colgan, S. W. J., & Erickson, E. F. 1996, ApJ, 465, 703  
 Ma, N. L., Smith, B. J., Radom, L., 1992, Chem. Phys. Lett., 197, 573  
 Mao, R. Q., Schulz, A., Zielinsky, M., Mauersberger, R., Störzer, H., Wilson, T. L., & Gensheimer, P. 2000, A&A, 358, 433  
 Mauersberger, R., & Henkel, C. 1991, A&A, 245, 457  
 Melo, V. P., Muñoz-Tuñón, C., Maíz-Apellániz, J., & Tenorio-Tagle, G. 2005, ApJ, 619, 270  
 Rodríguez-Rico, C. A., Viallefond, F., Zhao, J.-H., Goss, W. M., & Anantharamaiah, K. R. 2004, ApJ, 616, 783  
 Savage, C., & Ziurys, L. M. 2004, ApJ, 616, 966  
 Spaans, M., & Meijerink, R. 2007, ApJ, 664, L23  
 Strickland, D. K., & Heckman, T. M. 2007, ApJ, 658, 258  
 Rizzo, J. R., Fuente, A., Rodríguez-Franco, A., & García-Burillo, S. 2003, ApJ, 597, L153  
 Rizzo, J. R., Fuente, A., & García-Burillo, S. 2005, ApJ, 634, 1133  
 Usero, A., García-Burillo, S., Fuente, A., Martín-Pintado, J., & Rodríguez-Fernández, N. J. 2004, A&A, 419, 897  
 van der Tak, F. F. S., Aalto, S., & Meijerink, R. 2008, A&A, 477, L5  
 Weiß, A., Neiningner, N., Hüttemeister, S., & Klein, U. 2001, A&A, 365, 571  
 Wills, K. A., Redman, M. P., Muxlow, T. W. B., & Pedlar, A. 1999, MNRAS, 309, 395  
 Wilson, C. D., et al. 2007, A&A, 469, 121

## Appendix A: Rotational rate coefficients

For the rotational excitation of HCO<sup>+</sup> by hydrogen molecules, we employed the rate coefficients computed by Flower (1999). These rates are available for transitions between levels with  $J \leq 20$  and temperatures in the range  $10 \leq T \leq 400$  K. For HOC<sup>+</sup>, de-excitation rates were assumed identical to those of HCO<sup>+</sup> and the detailed balance principle was applied to derive the HOC<sup>+</sup> excitation rates. Note that these rates correspond to H<sub>2</sub> in its ground para level ( $J = 0$ ) and that rates for H<sub>2</sub> in excited rotational levels are not available.

Rate coefficients for electron-impact rotational excitation of HCO<sup>+</sup> and HOC<sup>+</sup> were computed using the *R*-matrix method combined with the Adiabatic-Nuclei-rotation (ANR) approximation. The *ab initio* *R*-matrix model of Faure & Tennyson (2001) for HCO<sup>+</sup> was employed here for all calculations on both molecular ions. The (theoretical) equilibrium geometry of HOC<sup>+</sup> was taken from Ma et al. (1992). A ground state dipole moment of 2.797 D was obtained, in excellent agreement with the value of 2.8 D computed by Defrees et al. (1982). The two lowest target states of symmetry <sup>1</sup>Σ<sup>+</sup> and <sup>3</sup>Π were included in the close-coupling calculation. Fixed-nuclei *T*-matrices were obtained for total symmetry <sup>2</sup>Σ<sup>+</sup>, <sup>2</sup>Π and <sup>2</sup>Δ, as in the case of HCO<sup>+</sup>. Full details about the *R*-matrix model will be published elsewhere.

The major difference with the calculations of Faure & Tennyson (2001) concerns the application of the ANR approximation. This latter has been recently shown to be valid down to threshold for molecular ions, provided a simple ‘‘Heaviside cor-

**Table 6.** Model Results (II)

| $A_v$<br>(mag) | $N(\text{CO}^+)$<br>( $\text{cm}^{-2}$ ) | $N(\text{HOC}^+)$<br>( $\text{cm}^{-2}$ ) | $N(\text{HCO}^+)$<br>( $\text{cm}^{-2}$ ) | $N(\text{CN})$<br>( $\text{cm}^{-2}$ ) | $N(\text{HCN})$<br>( $\text{cm}^{-2}$ ) | $N(\text{HCO})$<br>( $\text{cm}^{-2}$ ) | $N(\text{H}_3\text{O}^+)$<br>( $\text{cm}^{-2}$ ) | $N(\text{H}_2\text{O})$<br>( $\text{cm}^{-2}$ ) |
|----------------|--|---|---|--|---|---|---|---|
| M 82           | $1.5 \cdot 10^{13}$                      | $2.5 \cdot 10^{13}$                       | $1.1 \cdot 10^{15}$                       | $6.3 \cdot 10^{15}$                    | $1.1 \cdot 10^{15}$                     | $4.4 \cdot 10^{12}$                     | $1.1 \cdot 10^{14}$                               | $<2 \cdot 10^{14}$                              |
| 2              | $2.4 \cdot 10^{11}$                      | $4.5 \cdot 10^{11}$                       | $5.5 \cdot 10^{12}$                       | $1.7 \cdot 10^{12}$                    | $9.4 \cdot 10^{10}$                     | $2.1 \cdot 10^9$                        | $4.9 \cdot 10^{12}$                               | $4.7 \cdot 10^{13}$                             |
| 5              | $2.9 \cdot 10^{11}$                      | $5.7 \cdot 10^{11}$                       | $7.2 \cdot 10^{12}$                       | $1.4 \cdot 10^{14}$                    | $3.6 \cdot 10^{11}$                     | $3.7 \cdot 10^9$                        | $6.0 \cdot 10^{12}$                               | $6.6 \cdot 10^{13}$                             |
| 10             | $3.1 \cdot 10^{11}$                      | $6.2 \cdot 10^{11}$                       | $8.2 \cdot 10^{12}$                       | $6.6 \cdot 10^{14}$                    | $1.7 \cdot 10^{13}$                     | $4.4 \cdot 10^9$                        | $6.8 \cdot 10^{12}$                               | $1.1 \cdot 10^{15}$                             |
| 30             | $3.2 \cdot 10^{11}$                      | $6.7 \cdot 10^{11}$                       | $2.0 \cdot 10^{14}$                       | $1.4 \cdot 10^{15}$                    | $1.0 \cdot 10^{15}$                     | $2.1 \cdot 10^{12}$                     | $6.9 \cdot 10^{13}$                               | $4.8 \cdot 10^{16}$                             |
| 50             | $3.3 \cdot 10^{11}$                      | $7.1 \cdot 10^{11}$                       | $4.8 \cdot 10^{14}$                       | $1.8 \cdot 10^{15}$                    | $2.0 \cdot 10^{15}$                     | $7.8 \cdot 10^{12}$                     | $1.5 \cdot 10^{14}$                               | $1.0 \cdot 10^{17}$                             |
| 100            | $3.4 \cdot 10^{11}$                      | $8.0 \cdot 10^{11}$                       | $1.2 \cdot 10^{15}$                       | $2.9 \cdot 10^{15}$                    | $4.6 \cdot 10^{15}$                     | $2.2 \cdot 10^{13}$                     | $3.7 \cdot 10^{14}$                               | $2.4 \cdot 10^{17}$                             |

**Table 7.** Model Results (III)

|                                   | M82                  | 100% $A_v=5$ mag                      | 100% $A_v=10$ mag                       | 98.5% $A_v=5$ mag<br>1.5% $A_v=50$ mag |
|-----------------------------------|----------------------|---------------------------------------|---|--|
|                                   | M 82                 | No. clouds=44                         | No. clouds=40                           | No clouds=44                           |
| $N(\text{CO}^+)$                  | $1.5 \cdot 10^{13}$  | $1.3 \cdot 10^{13}$                   | $1.2 \cdot 10^{13}$                     | $1.3 \cdot 10^{13}$                    |
| $N(\text{HOC}^+)$                 | $2.5 \cdot 10^{13}$  | $2.5 \cdot 10^{13}$                   | $2.5 \cdot 10^{13}$                     | $2.5 \cdot 10^{13}$                    |
| $N(\text{HCO}^+)$                 | $1.1 \cdot 10^{15}$  | $3.2 \cdot 10^{14}$                   | <b><math>3.3 \cdot 10^{14**}</math></b> | $6.3 \cdot 10^{14}$                    |
| $N(\text{CN})$                    | $6.3 \cdot 10^{15}$  | $6.1 \cdot 10^{15}$                   | <b><math>2.6 \cdot 10^{16}</math></b>   | $7.2 \cdot 10^{15}$                    |
| $N(\text{HCN})$                   | $1.1 \cdot 10^{15}$  | <b><math>1.6 \cdot 10^{13}</math></b> | $6.8 \cdot 10^{14}$                     | $1.4 \cdot 10^{15}$                    |
| $N(\text{HCO})$                   | $4.9 \cdot 10^{13*}$ | <b><math>1.6 \cdot 10^{11}</math></b> | <b><math>1.7 \cdot 10^{11}</math></b>   | <b><math>5.3 \cdot 10^{12}</math></b>  |
| $N(\text{H}_3\text{O}^+)$         | $1.1 \cdot 10^{14}$  | $2.6 \cdot 10^{14}$                   | <b><math>2.7 \cdot 10^{14}</math></b>   | $3.6 \cdot 10^{14}$                    |
| $N(\text{H}_2\text{O})$           | $<2 \cdot 10^{14}$   | <b><math>2.8 \cdot 10^{15}</math></b> | <b><math>4.2 \cdot 10^{16}</math></b>   | <b><math>6.9 \cdot 10^{16}</math></b>  |
| $N(\text{CO}^+)/N(\text{HCO}^+)$  | 0.04                 | 0.04                                  | 0.04                                    | 0.02                                   |
| $N(\text{HCO}^+)/N(\text{HOC}^+)$ | 44                   | 12                                    | 13                                      | 25                                     |
| $N(\text{CN})/N(\text{HCN})$      | 6                    | 380                                   | 38                                      | 5                                      |

\* Average value in our HCO interferometric image (García-Burillo et al. 2002)

\*\* We mark in bold face those predictions that differ by more than a factor of 3 from the observed values

rection” is applied to excitation cross sections. Full details can be found in Faure et al. (2006). Note that closed-channel effects are neglected here as these are expected to be small for strongly polar ions (see Faure et al. 2006). Furthermore, in contrast to the calculations of Faure & Tennyson (2001) restricted to the lowest 3 rotational levels, we have considered here rotational transitions between levels with  $J \leq 20$  (i.e. involving rotational energies up to  $\sim 900$  K). Transitions were however restricted to  $\Delta J \leq 8$  owing to the limited number of partial waves included in the  $T$ -matrices ( $l \leq 4$ ). Finally, de-excitation rates have been fitted over the analytic form, Eq. (2), of Faure et al. (2004) for temperatures in the range  $5 \leq T \leq 1000$  K. Fitting coefficients for both HCO<sup>+</sup> and HOC<sup>+</sup> will be published in a forthcoming publication (Faure & Tennyson, in preparation). Note, finally, that the present HCO<sup>+</sup> rates have also been employed recently by Jiménez-Serra et al. (2006) to explain the overexcitation of HCO<sup>+</sup> in the shock precursor component of the young L1448-mm outflow.